Breakup Dynamics of Slender Bubbles in Non-Newtonian Fluids in Microfluidic Flow-Focusing Devices

Taotao Fu
State Key Laboratory of Chemical Engineering, School of Chemical Engineering and Technology, Tianjin University, Tianjin 300072, China

Laboratory of Reactions and Process Engineering, Nancy-University, CNRS, Nancy Cedex 54001, France

Youguang Ma
State Key Laboratory of Chemical Engineering, School of Chemical Engineering and Technology, Tianjin University, Tianjin 300072, China

Denis Funfschilling
Laboratory of Reactions and Process Engineering, Nancy-University, CNRS, Nancy Cedex 54001, France

Chunying Zhu
State Key Laboratory of Chemical Engineering, School of Chemical Engineering and Technology, Tianjin University, Tianjin 300072, China

Huai Z. Li
Laboratory of Reactions and Process Engineering, Nancy-University, CNRS, Nancy Cedex 54001, France

DOI 10.1002/aic.13723
Published online January 9, 2012 in Wiley Online Library (wileyonlinelibrary.com).

This study aims to investigate the breakup of slender bubbles in non-Newtonian fluids in microfluidic flow-focusing devices using a high-speed camera and a microparticle image velocimetry (micro-PIV) system. Experiments were conducted in 400- and 600-μm square microchannels. The variation of the minimum width of gaseous thread with the remaining time before pinch-off could be scaled as a power-law relationship with an exponent less than 1/3, obtained for the pinch-off of bubbles in Newtonian fluids. The velocity field and spatial viscosity distribution in the liquid phase around the gaseous thread were determined by micro-PIV to understand the bubble breakup mechanism. A scaling law was proposed to describe the size of bubbles generated in these non-Newtonian fluids at microscale. The results revealed that the rheological properties of the continuous phase affect significantly the bubble breakup in such microdevices. © 2012 American Institute of Chemical Engineers *AIChE J,* 58: 3560–3567, 2012
Keywords: bubble, breakup, non-Newtonian, flow-focusing, microfluidics, micro-PIV

Introduction

Recently, with the development of microchemical technology, microelectromechanical system and micrototal analysis technology, significant progress has been made in microfluidics.[1–3] Bubbles and droplets are frequently encountered in the various applications of microfluidics and usually generated by either a flow-focusing device or a microfluidic T-junction based on cross-flowing rupture technique.[4–8] Highly uniform bubbles and droplets can be produced by these methods. However, the mechanisms for bubble formation depend closely on the employed methods,[6,7,9] the flow rates of both phases, the geometry and size of microfluidic devices, as well as the properties of liquids.[5–20]

At low capillary numbers, gas bubbles formed in hydrodynamic flow-focusing liquids in a rectangular channel proceed through a linear collapse, followed by a fast unstable pinch-off.[5] During the collapse stage, the gaseous thread thins linearly with time, while during the unstable pinch-off, the minimum neck width and the time before breakup can be scaled with a power-law relation with an exponent of 1/3.[5] The size of formed bubbles is relevant to the gas and liquid flow rates as well as to the viscosity of the liquid phase.[6,21]

When bubbles generated in a microfluidic T-junction at low capillary numbers, the gaseous thread is squeezed by the accumulated pressure in the obstructed liquid phase and the thread neck thins linearly with time.[7] A recently experimental result showed that the breakup is initiated by the reverse liquid that flows from the thread tip to the neck where the pinch-off occurs.[22] The bubble size is proportional to the gas/liquid flow rate ratio.[7] At medium and high capillary numbers, the breakup process is also affected by the shear forces exerted on the thread and the resulting bubble, or droplet size is also relevant to the capillary number.[9,12]

Correspondence concerning this article should be addressed to Y. Ma at ygma@tju.edu.cn, and H. Z. Li at Huai-Zhi.Li@ensic.inpl-nancy.fr.

Most of above-mentioned works dealt with the bubble or droplet formation in Newtonian fluids, while many fluids for microfluidic applications are likely to exhibit complex non-Newtonian behaviors.[11,13,14,23,24] Moreover, the bubble dynamics in non-Newtonian fluids is of great fundamental interest and industrial relevance in such diverse domains as polymer devolatilization, fermentation, wastewater treatment, plastic foam processing, and metallurgy.[25] Some authors have investigated the effect of fluids' rheological properties on bubble or droplet formation and breakup mechanism in microfluidic devices. In a microfluidic T-junction, for the breakup of high molecular weight of polyethylene oxide (PEO) dispersed into Newtonian fluids, two distinct regions of filament-thinning dynamics were observed: a prestretch region and an exponential self-thinning region due to the elasticity of PEO solution, and the droplet size can be predicted based on force balance, concerning the shear, and drag forces, the inertia and interfacial forces.[11] In a microfluidic flow-focusing device, the elasticity of the dispersed phase can delay the filament thinning and breakup,[14,19] which could be divided into flow-driven regime and capillary-driven regime.[14]

The non-Newtonian character of continuous phases can also influence the bubble and droplet formation and breakup mechanism. For bubbles generated in gelatin solutions in a circular vertical tube coupled to a microfluidic device, the experimental results show that the flow patterns are mainly controlled by the gas and liquid flow rates, and the bubble size can be scaled with the gas/liquid flow rate ratio due to the inertial effect on bubble breakup.[16] For droplets formed in non-Newtonian fluids, the numerical results indicate that the rheology of the continuous fluid affects significantly the formation process and the size of droplets.[15] The droplet size decreases with the increase of apparent viscosity of continuous phase and can be predicted by an analytical model based on the force balance.[13] However, detailed information about the breakup mechanism of bubbles formed in non-Newtonian fluids in microfluidic devices is still missing until now.

This work aims at providing new insights into the bubble breakup mechanism in non-Newtonian fluids within microfluidic flow-focusing devices. The influence of fluid's rheological property on the bubble breakup dynamics was experimentally investigated.

Experimental Setup

The microfluidic devices were fabricated in a plate ($45 \times 27.5 \times 2$ mm^3) of polymethyl methacrylate (PMMA) by precision milling and sealed with another thin PMMA plate. The square sections were 600-μm wide $\times$ 600-μm deep and 400-μm wide $\times$ 400-μm deep (designated as +600 and +400, respectively). Stainless steel tubes ($d_i = 1$ mm) were used to connect the inlets and outlet of the microchannel to tygon tubes (inner diameter = 1.02 mm), which were used to connect the microchannel device with gas and liquid supplies. Gas was fed by a N_2 cylinder, and the gas flow rate was controlled by a high-precision micrometering valve (Sagana Instrumentation, Luxembourg). Liquid was delivered from a 60-mL syringe by a syringe pump (Harvard Apparatus, PHD 22/2000). The gas and liquid were introduced from the main channel and the two side channels, respectively. They met at the crossing section, which was located at 13.75 mm downstream of the inlets. When setting a new flow rate, the system was run for at least 300 s to reach steady state,

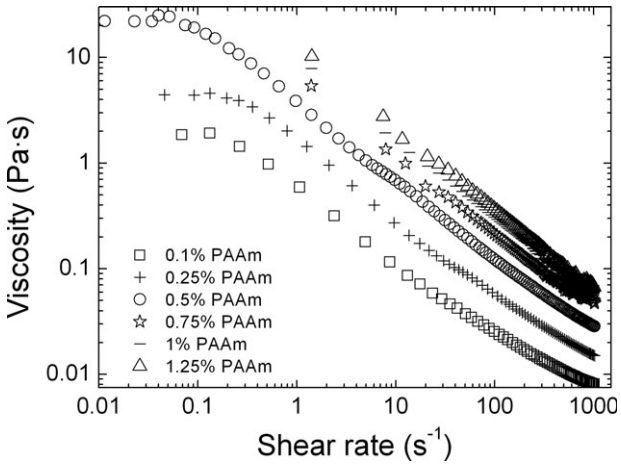

Figure 1. Rheological properties of PAAm solutions used.

verified by the camera visualization before measurements through two major parameters: the bubble formation frequency and the bubble size.[26] All of our experiments were conducted at room temperature and atmospheric pressure.

A high-speed camera CamRecord600 (up to 100,000 frames per second, Optronis GMBH, Germany) equipped a microscopic magnification lens mounted on an extension tube was set above the channel. A frame rate of 1000 fps and a shutter speed of 1/20,000 s were used. The resolution of the camera was 1280(H) $\times$ 512(V) pixels. A cold fiber light (Jeulin S.A., France) was placed at the other side of the channel to illuminate the channel. The images were processed by a Matlab program to obtain the quantitative features for bubbles.

A micro-Particle Image Velocimetry (micro-PIV) system (Dantec Dynamics, Denmark) was used by seeding the carrier fluid with 0.88-μm diameter calibrated Latex particles (Merck, France). The $\times$10 objective with a numerical aperture of 0.25 was used. The flow was illuminated by a stroboscope. By shadowgraph of the seeding particles, images of the flow were taken by a double image digital camera through the microscope at 2048×2048 pixels^2 resolution (1500×1500 μm^2). The measurements were realized on a slice of the microchannel of a value around 10 μm due to the focus of the microscope. The FlowMap software (Dantec Dynamics, Denmark) was used to analyze these raw image pairs, using an interrogation window size of 64×64 pixels^2 and a 50% window overlap. The images were processed by the cross-correlation function to compute velocity fields.

N_2 was used as the gas phase, and the flow rate was calibrated by a soap bubble flow meter at the inlet of the microdevice. Different concentrations of polyacrylamide (PAAm; SNF Floerger, France; 0.1–1.25 wt %) in demineralized water were used as non-Newtonian fluids. The surface tension was measured using a tensiometer, by the pendant drop technique on a Tracker apparatus (I.T. Concept, France). The contact angle of PAAm solutions on a flat PMMA surface varied from 44 to 67°. A Rheometric Fluid Spectrometer RFS II (Rheometric Scientific) was used to measure the rheological property of the liquids. They behaved as shear-thinning fluids and could be fitted by the power-law model in the range of the shear rates (1–500 s^{-1}) corresponding to the volumetric flow rates of the fluids (Figure 1)

Table 1. Physical Properties of PAAm Solutions Used

Fluid	Density, ρ_l (kg m^{-3})	Surface Tension, σ (mN m^{-1})	Consistency, K (Pa s^n)	Flow Index, n
0.1% PAAm	1000	71.0	0.34	0.49
0.25% PAAm	1000	70.3	1.05	0.41
0.5% PAAm	1000	69.6	2.87	0.36
0.75% PAAm	1000	69.3	4.32	0.34
1% PAAm	1000	67.7	7.91	0.29
1.25% PAAm	1000	67.2	10.85	0.26

$$\eta = K\dot{\gamma}^{n-1} \tag{1}$$

where η and $\dot{\gamma}$ are viscosity and shear rate, respectively; K is consistency, and n, flow index. The values of K and n are gathered in Table 1 for these fluids used.

Results and Discussion

Dynamics of breakup for slender bubbles

Different flow patterns: slug bubble, deformed slender bubble (missile bubble), annular, and intermittent flows were observed at the cross junction.[26] Slug bubble occurs at low gas and liquid flow rates (Q_g and Q_l, respectively). At medium liquid flow rate, deformed slender bubbles (missile bubbles) can be observed, and they are no longer in contact with the channel walls.

The typical formation processes for both slug and deformed slender bubbles (missile bubbles) in non-Newtonian fluids are shown in Figure 2. The breakup process for slug bubbles can be described by three stages: expansion, collapse, and pinch-off (Figure 2a), which is quite similar to the generation of slug bubbles in Newtonian fluids.[27] At the expansion stage, the gaseous thread expands in the radial direction and propagates in the axial direction, until the width of the thread reaches its maximum. Then, the gaseous thread experiences the collapse stage, during which, it continues to propagate in the axial direction and contracts in the radial direction. After a neck is formed, the focusing liquid flow pinches off the gaseous thread rapidly.

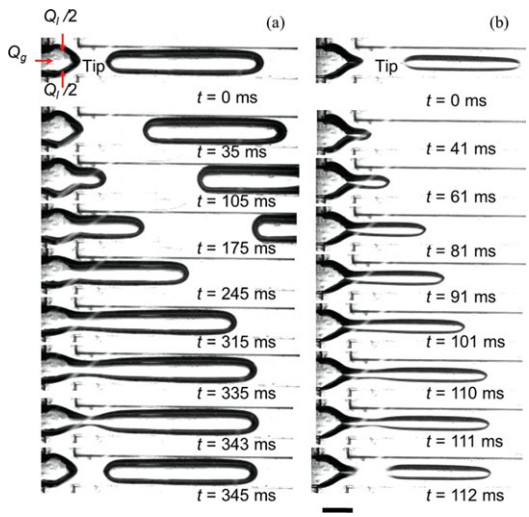

Figure 2. Optical micrographs of the evolution of periodic bubble formation process.

Liquid phase: 0.25 wt % PAAm. +600, scale bar: 600 μm. Q_g = 154 μL/min, (a) Q_l = 220 μL/min, T = 355 ms; (b) Q_l = 2200 μL/min, T = 112 ms.

For deformed slender bubbles (missile bubbles; Figure 2b), the gaseous thread is efficiently elongated by the focusing liquid. A cusp is observed at the rear of formed bubble, which is more visible for slender bubbles. This phenomenon was also found in conventional bubble columns at macroscale and can be attributed to the shear-thinning character of PAAm solutions.[28] In this case, the thread expands mainly in the axial direction, and a neck is formed after a certain moment. When its length exceeds the circumference, the thread becomes unstable and breaks up into bubbles.[29] After the pinch-off, the thread retracts. The deformation dynamics of the thread neck can give information for the bubble formation mechanism.[30] Therefore, the temporal evolution of the minimum width W_m for the gaseous thread during the thinning process is presented in Figure 3.

After having reached a plateau, the gaseous thread stretches for a certain period and then diminishes nonlinearly (Figure 3). This trend is similar to the bubble formation in Newtonian fluids: the thread first contracts linearly with time followed by a rapid nonlinear collapse.[8,27] In non-Newtonian fluids, the thread for slender bubbles is narrower than the square channel and is assumed to be axisymmetrical by the hydrodynamic flow-focusing fluids. It is a special 3-D case of the more general stability analysis of core-annular flow.[20] Dollet et al.[5] recently found that at small Reynolds numbers, the growth rate of the instabilities on the gaseous thread is positive, and the 3-D collapse is always unstable. The stretching phenomenon is peculiar for bubbles generated in non-Newtonian fluids in microfluidics. The shear-thinning fluids delay the final pinch-off of the gaseous thread, as the viscosity of the surrounding liquid varies with the local shear rate, which was

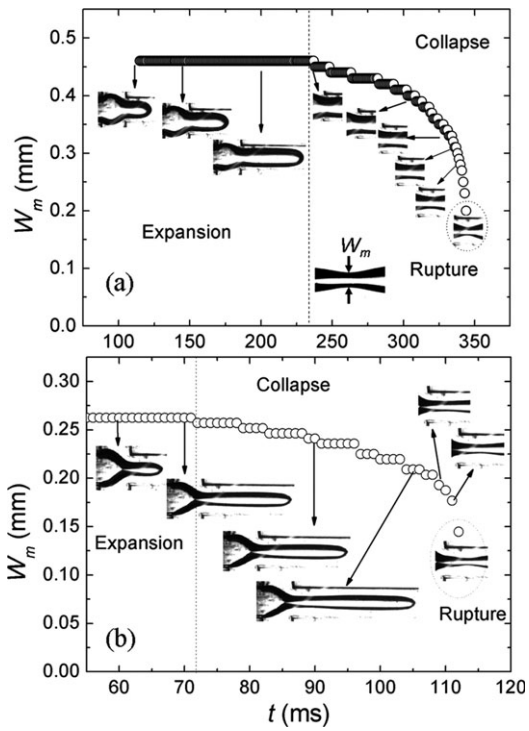

Figure 3. Temporal evolution of the minimum width of the gaseous thread during the thinning process, optical micrographs represent the variation of the thread neck, 0.25 wt % PAAm, Q_g = 154 μL/min, +600. (a) Slug bubble Q_l = 220 μL/min; (b) missile bubble Q_l = 2200 μL/min.

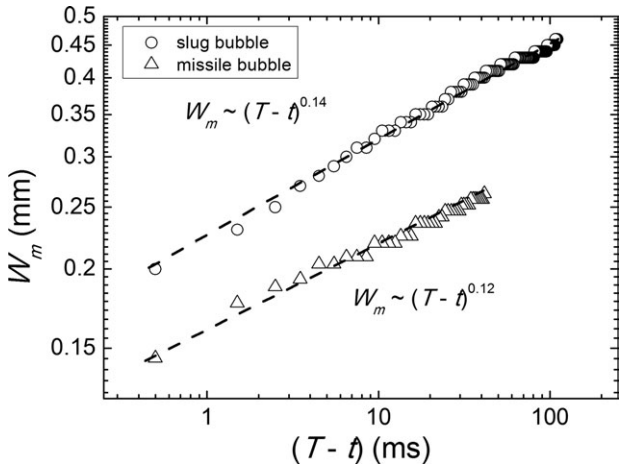

Figure 4. Scaling law for the minimum width of the gaseous thread during the collapse stage and W_m scaled with the remaining time ($T - t$) as a power-law relationship.

0.25 wt % PAAm, $Q_g = 154$ μL/min, +600. Slug bubble: $Q_l = 220$ μL/min; missile bubble: $Q_l = 2200$ μL/min.

verified by the calculation of the viscosity distribution in the liquid phase from the measured velocity field by the micro-PIV in the last part of the section. The delay of the bubble formation in shear-thinning fluids was also found in conventional columns, owing to a direct consequence of the deformation/relaxation of polymeric molecular.[31]

The physical mechanisms driving the collapse can be inferred from the behavior of the minimum width of the thread W_m just before breakup.[30,32] Thus, the minimum width of the thread W_m was plotted vs. the remaining time before breakup ($T - t$) (T is the bubble formation period, and t, the time). It is clear from Figure 4 that in +600, the minimum thread width exhibits power-law behavior before breakup: $W_m \sim (T - t)^{\alpha}$, with an exponent $\alpha = 0.14$ for slug bubble and $\alpha = 0.12$ for slender bubble (missile bubble). This power-law behavior is reminiscent of bubble formation in Newtonian fluids in either confined or unconfined systems in experimental, numerical, and theoretical studies.[5,21,30,32–36]

Similar behavior is observed for slender bubbles over a wide range of gas and liquid flow rates and concentrations of PAAm solutions (Figures 5 and 6). The analysis of these data leads to the mean power-law index of $\alpha = 0.14 \pm 0.05$ in 600 × 600 μm microfluidic device and $\alpha = 0.16 \pm 0.07$ in 400 × 400 μm microfluidic device. The differences of exponents between different kinds of bubbles and between different sizes of channels stem probably from the confinement effects on the gaseous threads in microchannels,[20] as the dimensionless maximum width of the slender gaseous thread neck W_o/W_c ranges between 0.26 and 0.8 in 600 × 600 μm microfluidic device and between 0.35 and 0.78 in 400 × 400 μm microfluidic device. While for slug bubbles, the dimensionless maximum width of the gaseous thread neck is usually greater than one. Furthermore, the exponent α is insensitive to the concentration of PAAm solutions (Figure 6), signifying a self-similar pinch-off phenomenon for the gaseous thread in various concentrations of PAAm solutions.[35]

It is necessary to mention that the power-law fittings obtained in the present experiment were conducted for the dimensionless minimum neck width W_m/W_c varying from 0.17 to 0.67 (W_m varying between 100 and 400 μm) in 600 × 600 μm microfluidic device and from 0.175 to 0.78 (W_m varying between 70 and 310 μm) in 400 × 400 μm microfluidic device. This variation range is comparable to that for the confined bubble pinch-off in Newtonian fluids in a microfluidic flow-focusing device performed by Dollet et al., in which W_m/W_c ranged from 0.25 to 1 (W_m varying between 5 and 20 μm).[5] However, for the bubble pinch-off in unconfined liquids, the dimensionless minimum neck width W_m/R_o (R_o is the diameter of the orifice for generating bubbles) varied from 0.085 to 0.8 (W_m varying between 228 and 2146

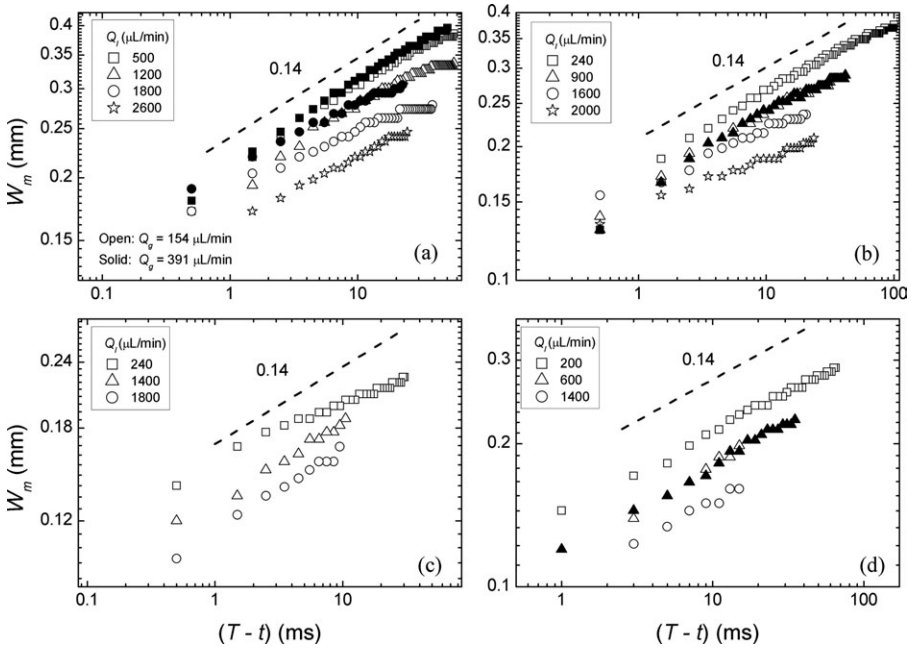

Figure 5. Relationship between minimum neck width W_m and remaining time ($T - t$) before pinch-off for various gas and liquid flow rates and concentrations of PAAm solutions: (a) 0.25 wt %; (b) 0.5 wt %; (c) 0.75 wt %; and (d) 1 wt %, +600.

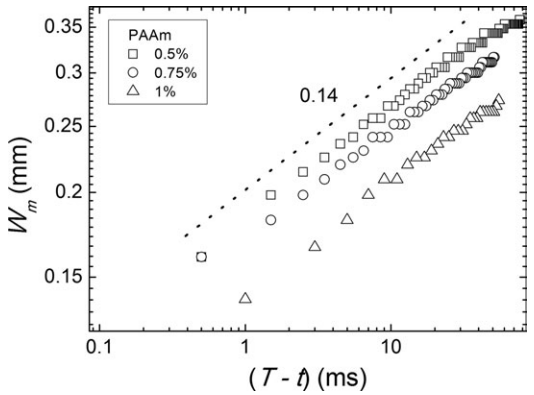

Figure 6. Effects of concentrations of PAAm solutions on the exponent α, +600.

μm) in the experiments[37,38] and from 0.081 to 0.35 (W_m varying between 220 and 500 μm) in the numerical studies[39]; Or, the rupture for the pinch-off of unconfined bubbles in water was found to occur, when the width of the gaseous thread neck reached 50 μm.[30]

Furthermore, the above-observed scaling relationships in the present experiments are different from those in Newtonian fluids either in confined or in unconfined systems. For example, the power-law relationship between the minimum thread width W_m and the remaining time before breakup ($T - t$) was found for unstable pinch-off stage for confined bubble formation in Newtonian fluids in microfluidic flow-focusing devices with an exponent $\alpha = 1/3$, where the collapse is mainly driven by both the gas and the liquid inertia, but not by the capillarity.[5,21] For gas bubbles formed in unconfined quiescent liquids, a power-law exponent $\alpha = 2/3$ was found, when inertia balances surface tension.[35] In the case of dominant viscous forces,[30] $\alpha = 1$ was observed in unconfined systems. Finally, for a purely inertial collapse in unconfined systems,[30,34] $\alpha = 1/2$. For the pinch-off of unconfined non-Newtonian power-law fluids, an exponent depending on the flow index n was usually found according to the asymptotic analysis and numerical computation.[40] Moreover, for the confined breakup of polymeric filaments in Newtonian fluids, an exponential thinning mechanism was observed experimentally.[11,14] The differences could be explained by a more complex equilibrium among three major forces involved: inertia, surface tension,[17,23,41] and in particular viscous forces depending on the local shear rate due to the shear-thinning character of PAAm solutions. The relative importance among these three forces during the bubble pinch-off were given by the local Reynolds number Re, the local Weber number We, and the local capillary number Ca defined as[33,42]

$$\begin{aligned} \mathrm{Re} &= \rho W_m \dot{W}_m/\eta \\ \mathrm{We} &= \rho W_m \dot{W}_m^2/\sigma \\ \mathrm{Ca} &= \eta \dot{W}_m/\sigma \end{aligned} \tag{2}$$

If the power-law relationship between the minimum width of the gaseous thread and the remaining time before breakup was assumed as $W_m \sim (T - t)^{\alpha}$, then the radial velocity of the interface could be expressed as $\dot{W}_m \sim \alpha (T - t)^{\alpha-1}$, and the local shear rate as $\ddot{W}_m \sim \alpha(\alpha - 1)(T - t)^{\alpha-2}$. And the local viscosity could be $\eta = K\ddot{W}_m^{n-1}$. Therefore, if the experimental scaling exponent is close to $\alpha = 0.14$ in 600 × 600 μm microfluidic device, it follows that $\mathrm{Re} \sim (T - t)^{1.86n-2.58}$, $\mathrm{We} \sim (T - t)^{-1.58}$, and $\mathrm{Ca} \sim (T - t)^{1-1.86n}$, with $n \in [0.26, 0.49]$. This signifies that Re and We divergence approaches the final pinch-off. Therefore, inertial forces dominate both viscous forces and surface tension.

It is worth noting that the magnitude of W_m depends on the gas and liquid flow rates as well on the concentration of PAAm solutions (Figures 5 and 6). As the power laws are scale-invariant, an extended scaling law was proposed as[29,40–42]

$$\frac{W_m}{W_c} = A\left(\frac{T - t}{T_c}\right)^{\alpha} \tag{3}$$

where the capillary time T_c is defined as $T_c = (\rho W_c^3/\sigma)^{1/2}$; and for +600, $T_c \approx 1.8$ ms, for +400, $T_c \approx 1$ ms. The prefactor A was found to relate to the capillary number of the liquid phase $\mathrm{Ca_l}$ ($\mathrm{Ca_l} = u_l' \eta_l'/\sigma$) (Figure 7) as: $A = 0.08\mathrm{Ca_l}^{-0.39}$

where

$$\begin{aligned} \eta_l' &= K\dot{\gamma}_l'^{n-1} \\ \dot{\gamma}_l' &= 3u_l'/(W_c - W_o) \\ u_l' &= Q_l/(W_c^2 - \pi W_o^2/4) \end{aligned} \tag{4}$$

are the non-Newtonian viscosity, characteristic shear rate,[14] and the liquid velocity, when the gaseous thread reaches its maximum width W_o. Furthermore, the capillary number $\mathrm{Ca_l}$ ranges from 0.008 to 0.1 in the present experiments. In view of these results, the breakup of the gaseous thread could be driven by increasing viscous stress, and an analogy would be drawn to some extent with the deformation of a slender bubble in non-Newtonian fluids in an extensional and creeping flow.[43]

The measurements of flow fields around the gaseous thread could give quantitative information about the role of liquid phase during bubble formation process.[22,27] Figure 8 illustrates an example of instantaneous velocity fields in the continuous liquid phase, during one period of bubble formation. At $t/T = 1/15$ (Figure 8a), the thread expands mainly in the axial direction, the liquid and gas flows almost do not influence mutually. At $t/T = 4/15$ (Figure 8b), the liquid flow is partly obstructed, and the liquid velocity around the thread neck decreases. At $t/T = 7/15$ (Figure 8c), the thread experiences the collapse stage. A visible neck is formed. At $t/T = 14/15$ (Figure 8d), the neck of the thread collapses at relatively high speed by the increasing focusing liquid.

It is necessary to mention that there is a stagnation zone in non-Newtonian fluids just on the outlet side of the flow

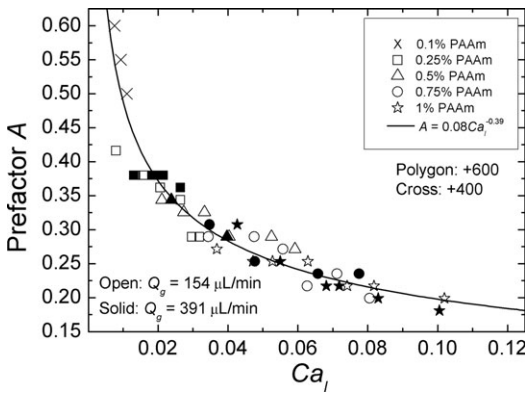

Figure 7. Relationship between the prefactor *A* and the liquid capillary number $\mathrm{Ca_l}$.

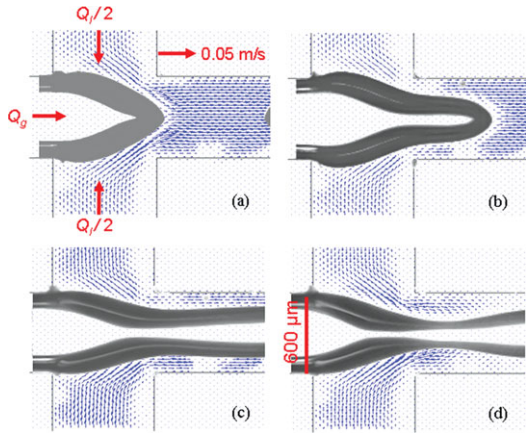

Figure 8. In-plane velocity fields in the continuous flow during one period of a bubble formation in the middle measurement plane, +600. Q_g = 154 μL/min; liquid phase: 1.25 wt % PAAm, Q_l = 70 μL/min.

(a) t/T = 1/15; (b) t/T = 4/15; (c) t/T = 7/15; and (d) t/T = 14/15. [Color figure can be viewed in the online issue, which is available at wileyonlinelibrary.com.]

focusing between the introducing liquid and a backflow due to the collapse of the bubble thread (Figure 9), this is not observed for bubble formation in Newtonian fluids.[27] Moreover, it is remarkable that the deviation of the size of the corner recirculation zone was observed in the two side arms of the microdevice, reflecting the unsteadiness degree in the time-dependent vortex dynamics.[44] The stagnation zone originates from the shape of the forming bubble as a consequence of the spatial distribution of non-Newtonian viscosity as shown in Figure 10. The liquid with low viscosity around the gas–liquid interface could delay the pinch-off of the bubble thread. This is probably one of the reasons for the exponent α less than 1/3 with respect to Newtonian fluids. Furthermore, it is also noteworthy that the back flow in the PAAm solutions (Figure 9) is caused by different pressures between the gaseous tip and neck, as reported for the breakup of confined bubbles at a microfluidic T-junction.[22]

From the results of micro-PIV measurement, the local shear rate was computed to obtain the viscosity distribution using Eq. 1 (Figure 10). The liquid viscosity varies almost 10-fold and is in the range of 1–10 Pa s. The viscosity is quite low near the gas–liquid interface in the cross junction due to the interplay of the gas and liquid flows. As in Figure 10c, the viscosity in the liquid phase between the thread and channel wall is quite high, which causes the slender shape of the bubble, that is, bubbles are not in contact with the channel walls. Close to the pinch-off point (Figure 10d), the viscosity around the neck decreases, delaying the bubble pinch-off. This might be another explanation for the exponent α less than 1/3. Moreover, the viscous stress distribution could also be estimated from Figure 10 and ranges between 2 and 32 Pa. As a plausible explanation, it is possible to argue that the shear-thinning character of the polymeric solutions used affects the bubble breakup dynamics via the spatial distributions of the viscosity and shear stresses. It also should be noted that the PAAm solutions have viscous fluid-like behavior as the Deborah number De is quite small (De is defined as the ratio of the characteristic time of fluid to the characteristic time of process).[31] For example, the relaxation time is about 10 ms for 1% aqueous solution of polyacrylamide,[31] and the typical flow time is about 300 ms (0.6 mm/2 mm/s) in the present experiment, resulting the Deborah number De of 1/30, quite less than one.

The influence of the PAAm solutions on the thread shape is illustrated in Figure 11. At the beginning of the bubble formation or just after the pinch-off (Figures 11a, b), higher concentration of PAAm solutions results in both sharper tip of the thread and sharper rear of the formed bubble. Furthermore, the higher the concentration of polymeric solution is, the stronger is the thread deformed (Figures 11c, d). These phenomena can be attributed to the greater stresses for higher concentration of PAAm solutions.

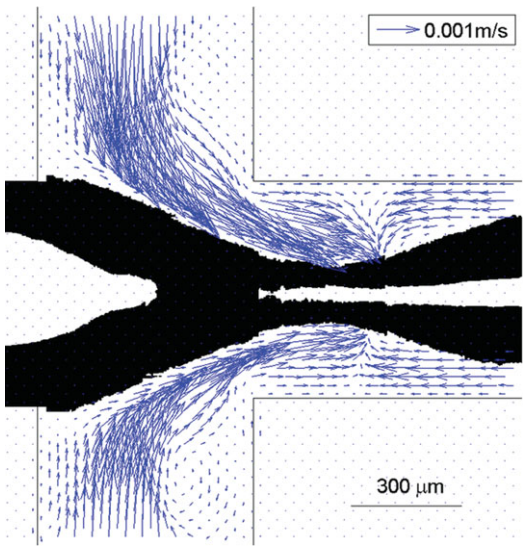

Figure 9. Contour and streamlines of velocity magnitude for the liquid phase around the gaseous thread before pinch-off at the measurement plane of 260 μm from the middle plane, +600.

Q_g = 154 μL/min; liquid phase: 1.25 wt % PAAm, Q_l = 70 μL/min. [Color figure can be viewed in the online issue, which is available at wileyonlinelibrary.com.]

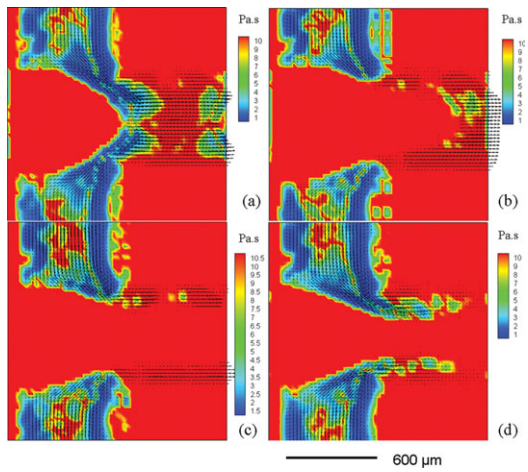

Figure 10. Viscosity distribution around the gaseous thread during one period of bubble formation in the middle plane, +600. Q_g = 154 μL/min; liquid phase: 1.25 wt % PAAm, Q_l = 70 μL/min.

(a) t/T = 1/15; (b) t/T = 4/15; (c) t/T = 7/15; and (d) t/T = 14/15. [Color figure can be viewed in the online issue, which is available at wileyonlinelibrary.com.]

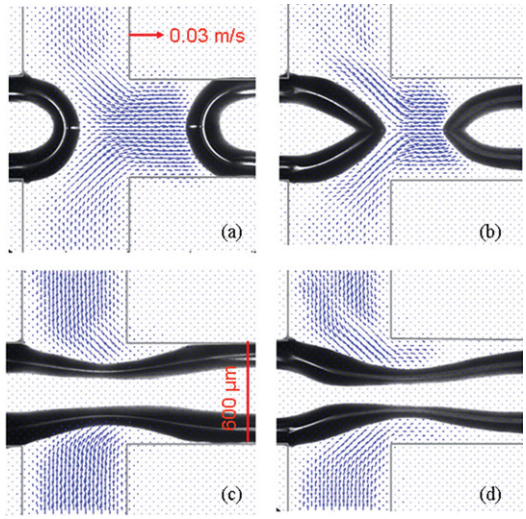

Figure 11. The shape of gaseous thread formed in different concentrations of PAAm solutions: (a) and (c) 0.1 wt % PAAm; (b) and (d) 1 wt % PAAm. Q_g = 154 μL/min, Q_l = 70 μL/min; (a) and (b) just after the pinch-off stage; (c) and (d) just before the pinch-off, +600.

[Color figure can be viewed in the online issue, which is available at wileyonlinelibrary.com.]

Scaling the bubble size

A dimensionless number is defined to quantify the bubble size: r/W_c r is the equivalent radius of the bubble: $r = (3V_b/4\pi)^{1/3}$. V_b is the bubble volume and was calculated directly from the captured images by a Matlab program on the assumption that the cross section of the bubble is circular: $V_b = \int \frac{\pi w^2(l)}{4} dl$, where l is the bubble length, and $w(l)$ is the bubble width at a certain l. It is found that the dimensionless bubble size r/W_c is almost proportional to the dimensionless maximum width of the thread neck W_o/W_c (Figure 12). This demonstrates that increasing the maximum width of the thread results in the formation of bigger bubbles.

As mentioned above, the deformation dynamics of the gaseous thread is influenced by the inertial effects and the spatial distributed viscosity with changing shear rates for PAAm solutions. Therefore, the bubble size varies with the gas/liquid flow rate ratio Q_g/Q_l for different concentrations of PAAm solutions in both microfluidic devices. As shown in Figure 13a, the bubble size augments with the increase of the flow rate ratio and with the decrease of the concentration of PAAm solutions. Moreover, the dimensionless bubble size could be scaled with the flow rate ratio as a power-law relationship (Figure 13a). The power law was also reported in the literature for bubbles generated in Newtonian fluids in capillary flow-focusing device[6] and in non-Newtonian fluids in microfluidic flow-focusing device.[16] In this work, a power-law relationship between the dimensionless bubble size and the flow rate ratio and the property of PAAm solutions could be fitted as follows

$$r/W_c = 1.51\left[\left(Q_g/Q_l\right)^{1-n}/K\right]^{0.28} \quad (5)$$

with a mean relative standard deviation of 7.63% (Figure 13b). Equation 5 can be used to predict the size of bubbles generated in shear-thinning fluids ($n \in [0.26, 0.49]$) in hydrodynamic flow-focusing microfluidic devices in a straightforward way, as it contains the gas/liquid flow rate ratio, the channel size,

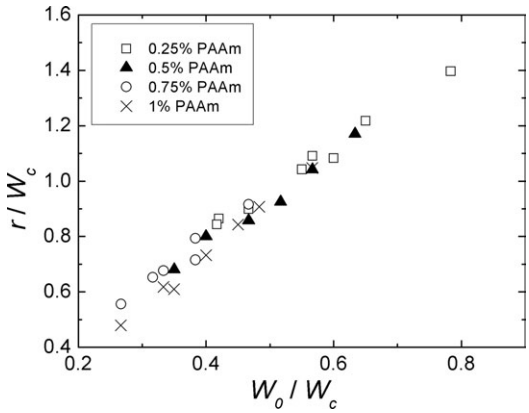

Figure 12. Relationship between the dimensionless bubble size and the maximum gaseous thread width. Q_g = 154 μL/min, +600.

and the liquid properties. However, for bubbles generated in gelatin solutions ($n = 0.45, 0.7, 0.95$) in a microfluidic device, a power law was found between the bubble size and the gas/liquid flow rate ratio with an exponent of 0.4, which was not highly sensitive to fluid properties.[16] The difference probably stems from the confinement effects on the bubble formation in microchannels,[20,27] as the exit has a narrow and short orifice which merges into a 2.75-mm circular tube in the experiment conducted by Skurtys et al.[16]

Alternatively, a power-law relation was also found for the bubble size by taking into account the flow rate ratio, the capillary number Ca_l, and the Reynolds number Re_l of the liquid phase:

$$r/W_c = 0.41\left(Q_g/Q_l\right)^{0.27(1-n)} Ca_l^{-0.33} Re_l^{-0.04} \quad (6)$$

with a mean relative standard deviation of 5.97%. The Reynolds number for the liquid phase is defined as: $Re_l = \rho_l U_l^{2-n} W_c^n / K$ and ranges from 0.002 to 2, where ρ_l, is the density. The superficial velocity is defined as $u_l = Q_l/W_c^2$. Equation 6 can be used to predict and analyze the size of bubbles formed in shear-thinning fluids in flow-focusing microfluidic devices with the involved forces such as the surface tension, the viscous forces, the inertia, and the pressure induced by the focusing liquid[26].

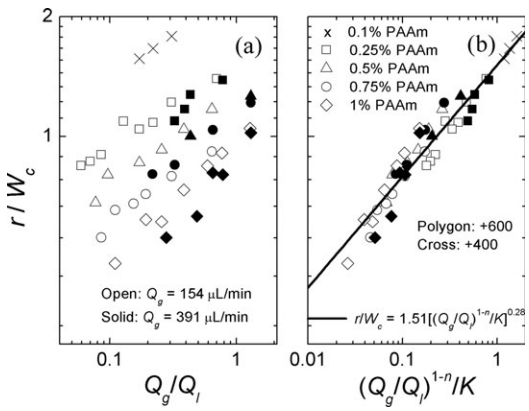

Figure 13. (a) Effects of flow rate ratio and concentrations of PAAm solutions on the bubble size; (b) scaling law of the bubble size in function of the gas/liquid flow rate ratio and the shear-thinning property of PAAm solutions.

Conclusions

The rheological properties of the PAAm solutions affect significantly the bubble breakup in microfluidic flow-focusing devices. The minimum width of the gaseous thread can be scaled with the remaining time before breakup as a power-law relationship with an exponent around 1/6 instead of 1/3 obtained for bubble pinch-off in Newtonian fluids.[5,21] The prefactor of the power-law relationship was related to the liquid capillary number. The velocity fields and the spatial viscosity distribution in the liquid phase, determined by the micro-PIV system, were used to explore the bubble formation mechanism. A scaling law was proposed to predict the bubble size, taking into account both the flow rate ratio and the rheological properties of PAAm solutions. This study could serve as the basis for further theoretical and experimental investigations, in particular the modeling and numerical simulation in microfluidics.[9,13,19]

Acknowledgments

The authors gratefully acknowledge the financial support for this project from the National Natural Science Foundation of China (Nos. 20876107 and 21076139), the aid of Opening Project of State Key Laboratory of Chemical Engineering (Grant No. SKL-ChE-08B06) and the Program of Introducing Talents of Discipline to Universities (Grant No. B06006). T. Fu appreciates the financial aid from both the China Scholarship Council and the French Embassy in China.

Literature Cited

1. Whitesides GM. The origins and the future of microfluidics. *Nature*. 2006;442:368–373.
2. Stone HA, Kim S. Microfluidics: basic issues, applications, and challenges. *AIChE J*. 2001;47:1250–1254.
3. Squires TM, Quake SR. Microfluidics:fluid physics at the nanoliter scale. *Rev Modern Phys*. 2005;77:977–1026.
4. Baroud CN, Gallaire F, Dangla R. Dynamics of microfluidic droplets. *Lab Chip*. 2010;10:2032–2045.
5. Dollet B, van Hoeve W, Raven J-P, Marmottant P, Versluis M. Role of the channel geometry on the bubble pinch off in flow focusing devices. *Phys Rev Lett*. 2008;100:034504.
6. Gañán-Calvo AM, Gordillo JM. Perfectly monodisperse microbubbling by capillary flow focusing. *Phys Rev Lett*. 2001;87:274501.
7. Garstecki P, Fuerstman MJ, Stone HA, Whitesides GM. Formation of droplets and bubbles in a microfluidic T-junction—scaling and mechanism of break-up. *Lab Chip*. 2006;6:437–446.
8. Garstecki P, Stone HA, Whitesides GM. Mechanism for flow-rate controlled breakup in confined geometries: a route to monodisperse emulsions. *Phys Rev Lett*. 2005;94:164501.
9. de Menech M, Garstecki P, Jousse F, Stone HA. Transition from squeezing to dripping in a microfluidic T-shaped junction. *J Fluid Mech*. 2008;595:141–161.
10. Tice JD, Lyon AD, Ismagilov RF. Effects of viscosity on droplet formation and mixing in microfluidic channels. *Anal Chim Acta*. 2004;507:73–77.
11. Husny J, Cooper-White JJ. The effect of elasticity on drop creation in T-shaped microchannels. *J Non-Newtonian Fluid Mech*. 2006;137:121–136.
12. Christopher GF, Noharuddin NN, Taylor JA, Anna SL. Experimental obervations of the squeezing-to-dripping transition in T-shaped microfluidic junctions. *Phys Rev E*. 2008;78:036317.
13. Sang L, Hong Y, Wang F. Investigation of viscosity effect on droplet formation in T-shaped microchannels by numerical and analytical methods. *Microfluid Nanofluid*. 2009;6:621–635.
14. Arratia PE, Gollub JP, Durian DJ. Polymeric filament thinning and breakup in microchannels. *Phys Rev E*. 2008;77:036309.
15. Qiu D, Silva L, Tonkovich AL, Arora R. Micro-droplet formation in non-Newtonian fluid in a microchannel. *Microfluid Nanofluid*. 2010;8:531–548.
16. Skurtys O, Bouchon P, Aguilera JM. Formation of bubbles and foams in gelatine solutions within a vertical glass tube. *Food Hydrocolloids*. 2008;22:706–714.
17. Pancholi K, Stride E, Edirisinghe M. Dynamics of bubble formation in highly viscous liquids. *Langmuir*. 2008;24:4388–4393.
18. Nie ZH, Seo MS, Xu SQ, Lewis PC, Mok M, Kumacheva E, Whitesides GM, Garstecki P, Stone HA. Emulsification in a microfluidic flow-focusing device: effect of the viscosities of the liquids. *Microfluid Nanofluid*. 2008;5:585–594.
19. Zhou CF, Yue PT, Feng JJ. Formation of simple and compound drops in microfluidic devices. *Phys Fluids*. 2006;18:092105.
20. Guillot P, Colin A, Utada AS, Ajdari A. Stability of a jet in confined pressure-driven biphasic flows at low Reynolds numbers. *Phys Rev Lett*. 2007;99:104502.
21. Fu T, Funfschilling D, Ma Y, Li HZ. Scaling the formation of slug bubbles in microfluidic flow-focusing devices. *Microfluid Nanofluid*. 2010;8:467–475.
22. van Steijn V, Kleijn CR, Kreutzer MT. Flows around confined bubbles and their importance in triggering pinch-off. *Phys Rev Lett*. 2009;103:214501.
23. Zhao C-X, Miller E, Cooper-White JJ, Middelberg APJ. Effects of fluid–fluid interfacial elasticity on droplet formation in microfluidic devices. *AIChE J*. 2011;57:1669–1677.
24. Nghe P, Terriac E, Schneider M, Li ZZ, Cloitre M, Abecassis B, Tabeling P. Microfluidics and complex fluids. *Lab Chip*. 2011;11:788–794.
25. Li HZ. Bubbles in non-Newtonian fluids: formation, interactions and coalescence. *Chem Eng Sci*. 1999;54:2247–2254.
26. Fu T, Ma Y, Funfschilling D, Li HZ. Gas–liquid flow stability and bubble formation in non-Newtonian fluids in microfluidic flow-focusing devices. *Microfluid Nanofluid*. 2011;10:1135–1140.
27. Fu T, Ma Y, Funfschilling D, Li HZ. Bubble formation and breakup mechanism in a microfluidic flow-focusing device. *Chem Eng Sci*. 2009;64:2392–2400.
28. Funfschilling D, Li HZ. Flow of non-Newtonian fluids around bubbles: PIV measurements and birefringence visualisation. *Chem Eng Sci*. 2001;56:1137–1141.
29. Eggers J. Nonlinear dynamics and breakup of free-surface flows. *Rev Modern Phys*. 1997;69:865–929.
30. Burton JC, Waldrep R, Taborek P. Scaling and instability in bubble pinch-off. *Phys Rev Lett*. 2005;94:184502.
31. Frank X., Li H.Z., Negative wake behind a sphere rising in viscoelastic fluids: a lattice Boltzmann investigation, *Phys. Rev E*. 2006;74:056307.
32. Basaran OA. Small-scale free surface flows with breakup: Drop formation and emerging applications. *AIChE J*. 2002;48:1842–1848.
33. Thoroddsen ST, Etoh TG, Takehara K. Experiments on bubble pinch-off. *Phys. Fluids*. 2007;19:042101.
34. Eggers J, Fontelos MA, Leppinen D, Snoeijer JH. Theory of the collapsing axisymmetric cavity. *Phys Rev Lett*. 2007;98:094502.
35. Day RF, Hinch EJ, Lister JR. Self-similar capillary pinchoff of an inviscid fluid. *Phys Rev Lett*. 1998;80:704–707.
36. Plesset MS, Prosperetti A. Bubble Dynamics and Cavitation. *Annu Rev Fluid Mech*. 1977;9:145–185.
37. Gordillo JM, Sevilla A, Rodriguez-Rodriguez J, Martinez-Bazan C. Axisymmetric bubble pinch-off at high Reynolds numbers. *Phys Rev Lett*. 2005;95:194501.
38. Chakraborty I, Biswas G, Ghoshdastidar PS. Bubble generation in quiescent and co-flowing liquids. *Int J Heat Mass Transfer*. 2011;54:4673–4688.
39. Quan S, Hua J. Numerical studies of bubble necking in viscous liquids. *Phys Rev E*. 2008;77:066303.
40. Doshi P, Suryo R, Yildirim OE, McKinley GH, Basaran OA. Scaling in pinch-off of generalized Newtonian fluids. *J Non-Newtonian Fluid Mech*. 2003;113:1–27.
41. Savage JR, Caggioni M, Spicer PT, Cohen I. Partial universality: pinch-off dynamics in fluids with smectic liquid crystalline order. *Soft Matter*. 2010;6:892–895.
42. van Hoeve W, Dollet B, Versluis M, Lohse D. Microbubble formation and pinch-off scaling exponent in flow-focusing devices. *Phys Fluids*. 2011;23:092001.
43. Favelukis M, Nir A. Deformation of a slender bubble in a non-Newtonian liquid in an extensional flow. *Chem Eng Sci*. 2001;56:4643–4648.
44. Lanzaro A, Yuan X-F. Effects of contraction ratio on non-linear dynamics of semi-dilute, highly polydisperse PAAm solutions in microfluidics. *J Non-Newtonian Fluid Mech*. 2011;166:1064–1075.

Manuscript received May 17, 2011, and revision received Dec. 1, 2011.